Three-dimensional micromagnetic domain structure of MnAs films on GaAs(001): Experimental imaging and simulations

R. Engel-Herbert and T. Hesjedal*
Magnetic Materials Laboratory, University of Waterloo, Waterloo, Ontario N2L 3G1, Canada

D. M. Schaadt
Paul-Drude-Institut für Festkörperelektronik, Hausvogteiplatz 5-7, D-10117 Berlin, Germany
(Received 23 August 2006; revised manuscript received 13 November 2006; published 27 March 2007)

The micromagnetic domain structure of MnAs films on GaAs(001) has been systematically investigated by micromagnetic imaging and simulations. The magnetic force microscopy (MFM) contrast resulting from the stray field of the simulated three-dimensional domain patterns was calculated and found to be in excellent agreement with MFM experiments. By combining three-dimensional stray-field imaging by MFM with surface sensitive probing and micromagnetic simulations, we were able to derive a consistent picture of the micromagnetic structure of MnAs. For example, the origin of the comblike contrast observed through MFM was identified as a metastable domain configuration exhibiting a cross-tie wall.

DOI: 10.1103/PhysRevB.75.094430 PACS number(s): 75.75.+a, 75.70.−i, 68.37.Rt

I. INTRODUCTION

In the analysis of magnetoelectronic structures, the primary goal of a magnetic imaging technique is to provide a spatially resolved picture of the magnetization throughout the sample or device.[1] Knowing the magnetic structure is at the heart of fabricating efficient magnetic devices, as properties such as magnetoresistance, the magnetic stray field, and magnetization reversal are all governed by the micromagnetic structure. This is true especially since the continuing increase in magnetic data storage density has led to the identification of magnetic elements with submicron lateral dimensions. At this length scale, the magnetization of soft ferromagnetic elements is generally either a vortex or a "single domain" state.[2] Despite the apparent simplicity of submicron-sized magnetic elements, there are a number of (meta)stable magnetic configurations possible, e.g., in Permalloy, that have to be taken into account before making practical use of these elements.[3]

For spin-based electronics,[4] which may rely on the injection of carriers across a ferromagnet-semiconductor interface, the epitaxial ferromagnet MnAs on semiconducting GaAs is a material system with interesting prospects.[5] With a Curie temperature above room temperature (~40 °C) and with GaAs as a superior optical and electronic material, spin-polarized carrier injection from MnAs into GaAs has been demonstrated.[6] MnAs-on-GaAs(001) exhibits a phase coexistence (10–40 °C) which is accompanied by the formation of alternating[7,8] submicron-wide ferromagnetic α- and nonferromagnetic β-MnAs stripes[9] due to the in-plane stress anisotropy.[10]

The commonly observed domain patterns were categorized based on their experimental observation by surface- and stray-field-sensitive microscopic imaging techniques, namely x-ray magnetic circular dichroism photoelectron emission microscopy (XMCD-PEEM) and magnetic force microscopy (MFM).[11,12] The three basic types are characterized by the number of domains on a single ferromagnetic α stripe along the effective easy axis direction. Recently, we have analyzed the thickness-dependent magnetization reversal of MnAs/GaAs(001).[12,13] We found that the magnetization states of MnAs in the easy plane, i.e., the basal plane of the hexagonal lattice, are an *S* and a Landau state leading to the observed type (I) domain, and a diamond and a double diamond state that are at the basis of the observed type (II) and (III) domains, respectively. These structures are shown in Fig. 3(d).

Here, we present a systematic analysis of the three-dimensional micromagnetic domain structure of MnAs by combining micromagnetic simulations and imaging. Complementary three-dimensional probing with MFM and surface-sensitive XMCD-PEEM gives a rather divergent picture of the magnetization. The derivation of the micromagnetic properties relying on one experiment alone results in a divergent magnetic picture of MnAs. The apparent discrepancies are due to the limits of the respective techniques and can be resolved by combining both techniques and micromagnetic simulations capable of calculating the MFM response.

II. THE MICROMAGNETIC STRUCTURE OF MnAs FILMS ON GaAs(001): EXPERIMENTAL OBSERVATIONS

The investigated single-crystalline MnAs samples were grown by molecular-beam epitaxy, as described elsewhere.[14,15] In the bulk, MnAs exhibits a uniaxial magnetocrystalline anisotropy with the *c* axis being the hard axis of magnetization.[16] The shape anisotropy of the film disfavors a magnetization normal to the film plane, leading to an effective magnetic easy axis behavior along the in-plane *a*-axis direction.[15,17] For the sample transport in a dry nitrogen atmosphere, an As cap was deposited. The XMCD-PEEM measurement described in Ref. 18 was carried out with an Elmitec microscope[19] at the Nanospectroscopy undulator beamline (ELETTRA, Trieste, Italy). For the desorption of the As cap, the samples were heated to ≈325 °C in the microscope's preparation chamber. After the complete desorption of the As cap, low-energy electron-diffraction patterns of

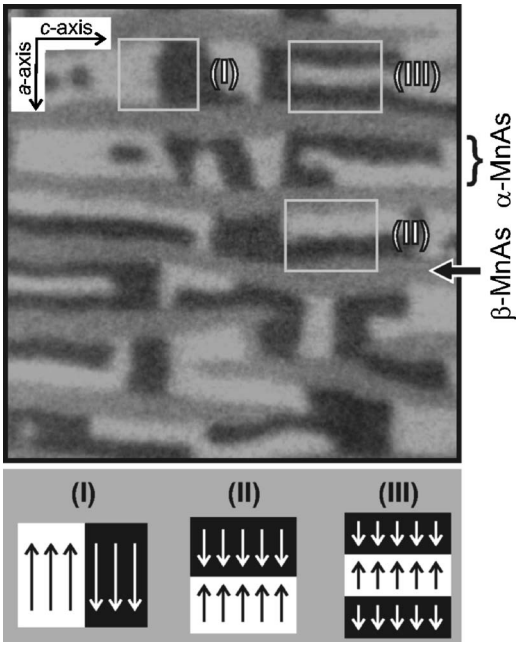

FIG. 1. 5×5 μm^2 image of the surface magnetization of a 120-nm-thick MnAs film obtained by XMCD-PEEM. The ferromagnetic α-MnAs stripes (dark and bright) are separated by nonferromagnetic β-MnAs stripes (gray, i.e., no magnetic contrast). The standard domain types are indicated in the image and illustrated below. Reprinted from Ref. 23, Fig. 2 (28 °C). Copyright Springer-Verlag 2006. With kind permission of Springer Science and Business Media.

MnAs $(\bar{1}100)(1\times2)$ were obtained. The samples were illuminated such that only the magnetization oriented along the *a* axis of MnAs (easy axis) was mapped. After XMCD-PEEM measurements, the samples were investigated by MFM in an ambient atmosphere using silicon nitride cantilevers sputter coated with Co/Cr (Veeco MSNC-MFMT). The tip radius was roughly 80 nm (measured by scanning electron microscopy) and, prior to the measurement, the cantilevers were magnetized along their tip axes to saturation.

A. Surface-sensitive imaging and the simple domain classification

XMCD-PEEM is a surface-sensitive magnetic imaging technique that combines x-ray absorption spectroscopy and electron microscopy.[20] The contrast formation originates from the difference in x-ray absorption coefficients depending on the relative orientation of photon helicity and magnetization. The secondary electron yield is proportional to the absorption coefficient and the emitted electrons are detected in PEEM. The lateral resolution of this quantitative imaging technique is about 10–20 nm.[21]

Figure 1 shows a 5×5 μm^2 XMCD-PEEM image of a 120-nm-thick MnAs film on GaAs(001) recorded at 28 °C (the stripe width is a function of temperature). The contrast corresponds to the projection of the surface magnetization onto the vector of the incident light along the effective easy axis, i.e., the *a* axis as indicated in Fig. 1. The α-β-stripe structure is clearly visible as gray (β-MnAs, no magnetic contrast) and dark (bright) areas (ferromagnetic α-MnAs). On the ferromagnetic stripes, three different domain patterns are found that are classified depending on the number of domains along the easy *a*-axis direction (perpendicular to the stripe). Examples of the domain patterns are labeled in the figure accordingly. Below, the magnetization patterns associated with the three domain types are sketched. Without micromagnetic simulations it is possible to suspect the formation of head-to-head domains at the basis of the domain types (II) and (III). Head-to-head domains are known to exist in thinner films due to the less severe energy penalty associated with the magnetic charges on their walls.[22] On the contrary, type (II) and (III) domains are found in MnAs for thicker films ($\gtrsim$100 nm) only. Here, one should rather expect an underlying three-dimensional magnetization pattern that leads to "apparent" head-to-head domains. In the Sec. II B, we demonstrate how MFM imaging can shed light on the three-dimensional magnetization of the film.

B. Stray-field imaging—MFM

The MFM is a variant of the scanning force microscope family capable of recording the magnetostatic force or force gradient between the magnetic tip and a magnetic sample. The advantage of this technique is that it also operates in an ambient condition and no special sample preparation is required.

The interpretation of the measured MFM signal is not straightforward, since the magnetization distribution is not monitored directly. Instead, the stray-field emanating from the sample—which naturally reflects the three-dimensional sample magnetization—determines the MFM contrast. Thus, the simulation of the contrast based on a given sample magnetization is a necessity for making full use of the MFM data, as will be discussed in detail in Sec. IV.

The MFM image shown in Fig. 2(a) was recorded at a temperature of 18 °C with a temperature-controlled MFM setup.[24] Prior to the measurement, the sample was heated above the phase transition temperature to start from a completely demagnetized state. The position of the ferromagnetic α- and nonferromagnetic β-stripes are indicated on the right-hand side. On the α stripes, and also slightly extending into the β-phase region, magnetic contrast (bright) originating from the stray field of the sample is found. Alternating type (I) domains give rise to a meanderlike contrast [labeled (I)]. The type (II) domain labeled in the figure is characterized by a bright area in the middle of the stripe and two narrow lines right at the stripe edges. A type (III) domain that corresponds to the surface magnetization shown in Fig. 1 below is indicated on a wider α stripe. Further, comblike domain patterns are frequently observed. They occur in two subtypes, C(I) and C(II), which are characterized by longer and shorter hooklike features extending from a bright area near the edge and the middle of the stripe, respectively. They are closely related to the standard type (I) and (II) domains, as will be shown in Sec. V.

The interaction of the magnetized tip with the stray field of alternating type (I) domains is illustrated in Fig. 2(b). For

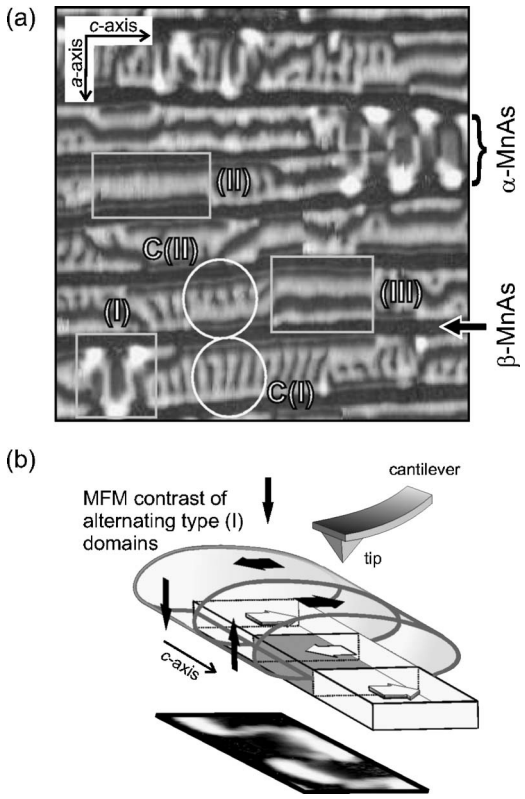

FIG. 2. (a) 5×5 μm^2 image of the stray field of a 180-nm-thick MnAs film obtained by MFM at 18 °C. Besides the standard domain types (rectangular markers), comblike structures are found (circular markers) that are labeled C(I) and C(II) referring to their connection to type (I) and (II) domains, respectively. (b) Sketch illustrating the contrast mechanism in MFM. Bright contrast corresponds to an attractive interaction between tip and sample and dark contrast to a repulsive interaction.

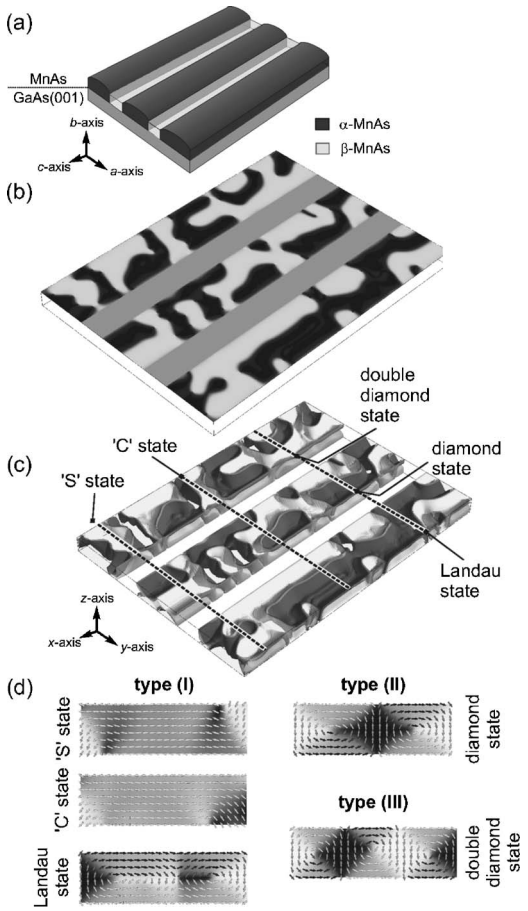

FIG. 3. Sketch of (a) the α-β-stripe structure of a MnAs film on GaAs(001) and (b) the simulated surface magnetization. (c) Isosurface plot (for ten constant M_y values) of the three-dimensional magnetization distribution. (d) Cross-sectional magnetization patterns are shown at the positions indicated in (c). The arrows indicate the magnetization in the basal plane. Their grayscale corresponds to the M_y component, and the underlying image to the M_z component of the magnetization. The stripe geometry corresponds to a sample temperature of 28 °C.

simplicity of the discussion, we assume a sequence of oppositely magnetized bar magnets. The stray field of the bar magnets will now either point out of the plane or into the plane at the edges of the ferromagnetic stripe. The relative orientation of the tip magnetization and the out-of-plane component of the sample stray field (at the scan height) determine the tip-sample interaction. The parallel (antiparallel) orientation of the two magnetization vectors results in an attractive (repulsive) interaction, giving a bright (dark) contrast. Additionally, 180° Bloch walls show up as bright or dark lines separating areas of opposite magnetization. The resulting MFM contrast (experimental) is shown below the sketch [Fig. 2(b)]. As the MFM image was obtained in conventional noncontact mode, and not in the so-called lift mode, the magnetic contrast does not range from dark to bright as expected [cf. Fig. 2]. In lift mode, each line is scanned twice, once for determining the topography of the sample and then for measuring the additional tip-sample interaction at this height. Instead, due to the mixing with the van der Waals force in noncontact mode, the lowest contrast level is usually found to coincide with the nonferromagnetic areas.[25]

Although there are a number of similarities between the domain picture obtained from surface-sensitive XMCD-PEEM and stray-field-sensitive MFM, e.g., in general, the same number of domain types are found with both methods, the micromagnetic picture of MnAs obtained so far is rather divergent.[26] For instance, C(I) and C(II) domains are not seen in XMCD-PEEM imaging. On the other hand, in MFM no extended type (I) domains can be found. In order to find the magnetization distribution that is able to satisfy both experimental observations, we performed micromagnetic simulations.

III. THE MICROMAGNETIC STRUCTURE OF MnAs FILMS ON GaAs(001): SIMULATIONS

We present the simulated magnetization distribution of a 120-nm-thick MnAs film at a temperature of 30 °C.[27] Following the experimentally derived temperature dependence of the α-β-phase ratio [cf. Fig. 3(a)],[23] the ferromagnetic α-phase stripe width was set to 384 nm and the β-phase stripe width to 192 nm. The exchange constant A is assumed

to be 1.0×10^{-11} J/m and the saturation magnetization M_s =800 kA/m.[12] These are reasonable values within the range of reported parameters from below 400–1100 kA/m.[28,29] Bulk MnAs, in comparison, has 670 kA/m. These parameters give an exchange length of L_{ex}=5 nm, where L_{ex} is defined as $\sqrt{2A/(\mu_0 M_s^2)}$. A magnetocrystalline anisotropy constant of $K=-7.2\times10^5$ J/m^3 was chosen for MnAs,[12] in agreement with superconducting quantum interference device (SQUID) magnetometry[15] and ferromagnetic resonance measurements.[17] In accordance with the experimental procedure, where the sample was heated to the complete nonferromagnetic β-phase[9] prior to measurement, a fully randomized initial magnetization was assumed for the α stripes.

The employed finite difference code is based on the Landau-Lifshitz-Gilbert equation (LLG). For obtaining the relaxed, i.e., minimum-energy configuration, we applied a self-consistent approach. The momentary magnetization distribution describes a damped precession around its effective magnetic field, which provides a torque acting on the magnetization. The damping aligns the magnetization with the effective magnetic field. Through repetition, the total energy is minimized until a given limit for the energy difference between two subsequent energy states is reached. Details of the parallel, three-dimensional computing code are discussed elsewhere.[30] For the presented problems, we use a cell size of 8 nm. Although it is in general preferable to choose a cell size that is equal or smaller than the exchange length, we had to find a compromise between the real exchange length and the computational demands in terms of addressable memory and computation time. This cell size is still acceptable for the problem of extended stripes. Although the surface magnetization pattern appears rather simple [cf. Fig. 3(b)], in correspondence with the XMCD-PEEM experiments, the three-dimensional magnetization distribution [cf. Fig. 3(c)] deserves further attention.

The observed domain patterns are classified following the scheme presented in Ref. 11. The in-depth magnetization distribution that is at the basis of the simple, surface-based classification scheme is visualized in Fig. 3(d). In the cross section, visualizing the magnetization distribution in the basal plane, typically five magnetization patterns are found. Type (I), defined by a homogeneous magnetization across the width of the stripe, can have three underlying patterns: the *S* state, the *C* state, and the Landau state. The *S* and *C* states are characterized by a predominant uniform magnetization in the easy axis, with deviations at the opposite or lower corner points, respectively. The Landau state is a flux-closure pattern with opposite magnetization in the upper and lower half of the cross section. In the presented case, the magnetization further shows a cross-tie wall as will be explained below. The nomenclature is in accordance with magnetization patterns observed in soft magnetic thin film elements.[22] Interestingly, and in contrast to their observation in the film plane of soft ferromagnetic elements, they appear in MnAs thin films in the basal plane, i.e., perpendicular to the surface. The strong magnetocrystalline anisotropy of MnAs and its planar symmetry prevents a magnetization along the *c* axis, similar to the effect of the shape anisotropy in soft magnetic thin film elements. Generally, these patterns are flux-closure patterns.

For a convenient discussion of the results, we introduce a Cartesian coordinate system with the *z* axis being the film normal, as illustrated in Fig. 3(c). The magnetization components M_x, M_y, and M_z are the respective components of the magnetization vector normalized to saturation magnetization M_s.

A. Common domain patterns: The type (I), (II), and (III) domains

For simulating the observed standard domain types, we start from the respective cross sections (cell dimensions: 48 $\times$15 cells) found in the simulation of the coupled stripe array [shown in Fig. 3] and duplicate them along the *c*-axis direction for 110 cells, i.e., 880 nm. The magnetization patterns are then allowed to relax and the results are shown in Fig. 4.

First of all, we found type (I) domains based on the *C* and *S* states not stable upon relaxation of the extended structure for the given combination of geometry and saturation magnetization. The reason is the large demagnetization energy that leads to the stabilization of other domain types which will not be further discussed in this context. Of course, extended type (I) domains can become stable in narrower ferromagnetic stripes or in coupled stripe arrays. Thus, we assumed a different initial magnetization which is found in experimental MFM images [cf. Fig. 2]. This alternating sequence of type (I) domains is stable upon relaxation and shown in Fig. 4(a). The type (II) and (III) domains, which originate from one and two extended diamond-shaped cross-sectional domains, respectively, are shown in Figs. 4(b) and 4(c). All three domain patterns are in agreement with the observed XMCD-PEEM contrast representing the surface magnetization.

Table I lists the calculated total energies E_{tot}, the exchange energies E_{exch}, and the demagnetization energies E_{demag} for all domain types in reduced units. Since the magnetization along the *c* axis is negligible for all domain types, the anisotropy energy has been omitted. Its value never contributes more than 1% to the total energy. The lowest total energy for the extended domains is found for the type (III) domain, closely followed by the type (II) domain. The type (I) domain has by far the largest total energy. The exchange energy is increasing from type (I) over (II) to (III). Type (I) domains have a small exchange energy, since only the Bloch walls and the deviation of the magnetization at the edges contribute to this value. In the case of type (II) and (III) domains, the values are about twice as large, since closure-domain patterns involving a large number of domain walls are present. As a consequence, the demagnetization energy is considerably smaller. Interestingly, for the type (I) domain, the demagnetization energy is large although the sequence of oppositely magnetized domains reduces the demagnetization energy of the system significantly.

B. Unique domain patterns

Besides the classified structures discussed in Sec. III A, there exist a multitude of domain patterns that can be, on first sight, explained as a combination of the three basic

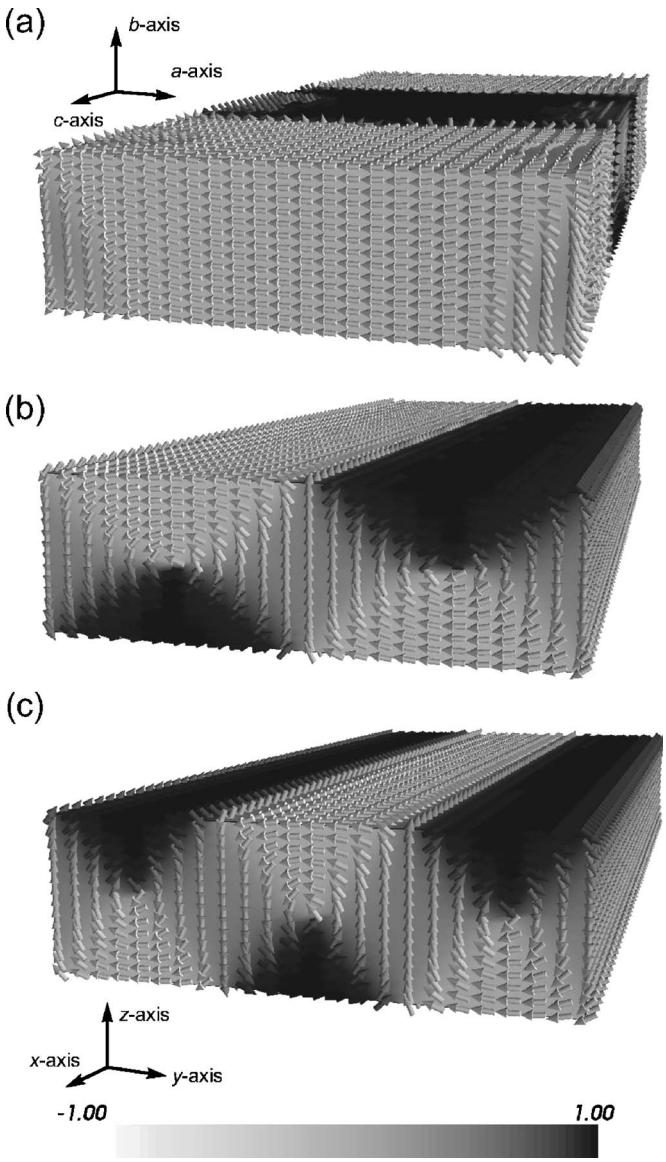

FIG. 4. Magnetization distribution for the relaxed, extended standard domain types (I), (II), and (III). The grayscale represents the value of the in-plane magnetization component M_y. The surface contrast corresponds to the magnetization distribution observed in XMCD-PEEM images. The stripe width is observed at a sample temperature of 28 °C.

structures.[11] As the α stripe width that corresponds to a certain temperature only reflects an average width, we also investigated wider α stripes.[31] A typical variation of the stripe width can be seen in both experimental images [Figs. 1 and 2]. Deviations from the simple domain scheme, shown in Fig. 3, can be explained by a variation of the α-stripe width. Two prominent examples are deviations from the ordinary type (II) domain structure. For type (II) structures, the existence of a single symmetric diamond state in the basal plane is no longer energetically favorable. Instead, the system has to stabilize the spin configuration by the introduction of additional features. One is characterized by the formation of zigzag-shaped walls (along the c axis) in the middle of the α stripe.[18] In the underlying diamondlike structure, the diamond is periodically skewed looking along the stripe axis (c axis).

TABLE I. Energies for the relaxed, extended standard domain types. The total energy E_{tot}, the exchange energy E_{exch}, and the demagnetization energy E_{demag} are given in reduced units, i.e., normalized to $\mu_0/2 \cdot M_s^2 = 3.77 \times 10^5$ J/m^3.

	E_{tot}	E_{exch}	E_{demag}
Type (I)	14.0×10^{-2}	2.27×10^{-2}	11.5×10^{-2}
Type (II)	8.30×10^{-2}	4.62×10^{-2}	3.71×10^{-2}
Type (III)	8.06×10^{-2}	5.04×10^{-2}	3.02×10^{-2}

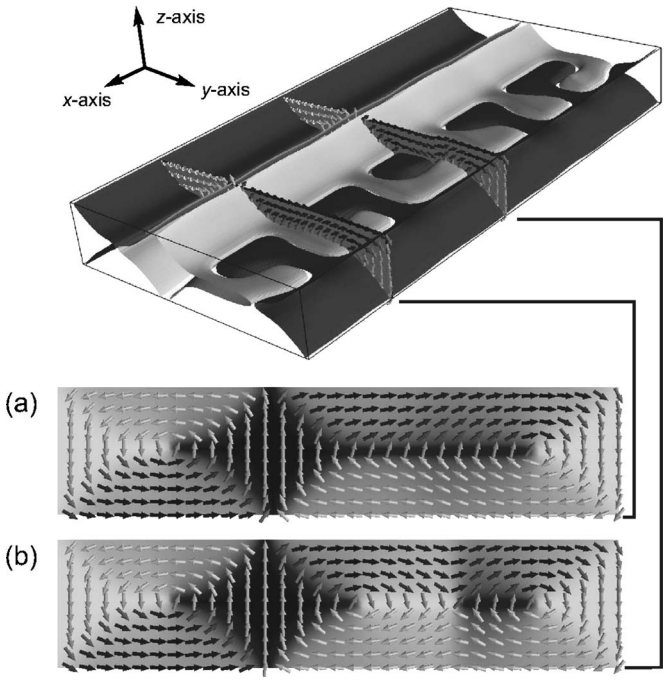

FIG. 5. Magnetization pattern of the comblike domain structure. The isosurfaces of the normalized magnetization ($M_y = M_x = \pm 0.707$) illustrate transitions from in-plane to out-of-plane oriented magnetization vectors. At selected positions, cross-sectional cuts are shown below in (a) and (b). The underlying grayscale corresponds to the out-of-plane component M_z, whereas the gray value of the arrows represents the in-plane component M_y. The stripe width corresponds to a sample temperature of 18 °C.

Another unique domain pattern is characterized in MFM by a comblike contrast (see Fig. 2). As the zigzag-shaped wall was investigated in detail in Ref. 18, we will focus on the discussion of the origin of the comblike domain pattern. To take wider stripes into account, we simulated the magnetization pattern for a width-to-thickness ratio of 4.27 instead of 3.13. This corresponds to a sample temperature of 18 °C instead of 28 °C.

Figure 5 shows the underlying magnetization distribution that leads to a type (II) domain on the surface and to the comblike contrast in MFM. Isosurfaces of the magnetization component $M_z = \pm 0.707$ are shown as bright and dark, respectively. The chosen value of 0.707 indicates the isosurface where both the in-plane component M_y and the out-of-plane component M_z are equal. The magnetization pattern

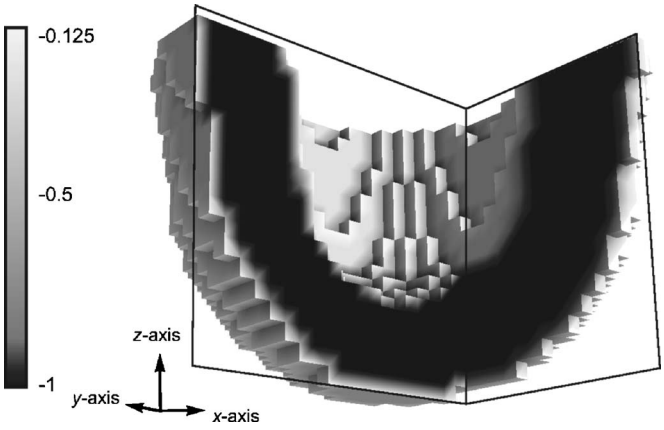

FIG. 6. Illustration of the tip magnetization used for the MFM simulations. The scale represents the relative magnitude of the normalized magnetization component M_z.

is governed by a diamond structure that is not centered, as common in type (II) patterns, but shifted toward one edge of the stripe. The diamond pattern branches off in the middle of the stripe (in depth) and forms hook-shaped extensions. Within the volume of the hooks, the magnetization is out-of-plane, leading to an enhanced MFM signal. At selected positions in the comb structure, cross-sectional views are shown in Figs. 5(a) and 5(b). The first position is taken along the base of an extension and the second cut across the hook-shaped tail of the protrusion. The "hooks" are found to extend in both the $+x$ and $-x$ directions. Along the base of the extension [cf. Fig. 5(a)], an elongated Néel wall is found. The second cross section [Fig. 5(b)] across the end of the hook-shaped structure reveals a diamond state, too. In addition, instead of an elongated Néel wall, a complicated composite wall is apparent. The domain transition is of cross-tie wall character, consisting of Bloch and Néel wall-like segments. The rotation sense of the Néel wall is changed, introducing the Bloch wall-like segment.[22]

IV. SIMULATION OF THE MAGNETIC FORCE MICROSCOPY RESPONSE

A. Description of the magnetic force microscopy simulation tool

The MFM contrast was obtained from a micromagnetic simulation of the tip-sample system assuming mutual nondisturbance and a realistic tip model. Typical MFM tips are made from Si and sputter coated with a magnetic layer, e.g., Co. Thus, the tip was modeled as a hollow cone with a spherically shaped apex.[25] The discretization of the tip-sample volume was 6 nm in all three dimensions. The tip has a radius of curvature of 80 nm, a side angle of 10°, and a magnetic coating thickness of 40 nm. Since in MFM experiments the tip is fully magnetized to saturation in the z direction (i.e., along the tip axis), we modeled the tip to have a constant magnetization in the $-z$ direction. The tip magnetization was not relaxed to its equilibrium state. The tip's height was truncated after 20 layers, and the employed tip model is shown in Fig. 6. The grayscale corresponds to the magnitude of the magnetization component M_z and reaches from -1 (dark) to -0.125 (bright). To approximate the tip better without increasing the number of cells, the magnetization of the near-surface cells was weighted by the number of corner points that are part of the magnetic coating. The tip of finite size is placed at a constant height of 30 nm above the sample. The complete MFM image is obtained by raster scanning the tip across the sample in discrete steps and calculating the force gradient of the magnetostatic interaction at each scan position. Thus, the calculated MFM contrast corresponds to the signal obtained in lift-mode MFM. Thus, it does not account for the van der Waals interaction which gives rise to the unavoidable topographic contrast in noncontact force microscopy. As the MFM image (cf. Fig. 2) was not obtained in the so-called lift mode, the measured contrast is a convolution of the topography-induced and magnetic interactions. A detailed description of the MFM response simulation procedure is given in Ref. 25.

B. Results for the standard domain patterns

For the MFM response calculation, the ferromagnetic stripes presented in Fig. 4 were sandwiched between six cells of nonferromagnetic material. This extension is necessary to capture the MFM contrast that is not limited to the position of the sample. Figure 7(a) shows the MFM response (force gradient) for three oppositely magnetized, neighboring type (I) domains obtained from micromagnetic simulations [cf. Fig. 4(a)]. The contrast is dominated by dark and bright areas located on opposite positions on the stripe. Interestingly, the MFM contrast extends over the edges of the stripe, indicated by the dotted lines. This is also found for the experimental MFM images [cf. Fig. 2(a), type (I) domains]. The 180° domain walls separating the oppositely magnetized areas are of the Bloch type. Both Bloch walls are partly bright and dark, showing that the magnetization rotates through the out-of-plane direction in the positive or negative sense. This behavior is in accordance with the experimentally observed Bloch walls. The contrast originating from the Bloch walls is smaller than for the domains.

In Fig. 7(b), the MFM contrast for the type (II) domain is depicted [cf. Fig. 4(b)]. The contrast on the opposite sides of the stripe is the same (dark) and the force gradient is stronger than that of the bright area in the middle of the stripe. This means that the stray-field contrast from the edges of the stripes is stronger than the influence of the extended diamond structure with its out-of-plane moments in the middle of the stripe. Furthermore, a slight modulation of the contrast is visible along the stripe, e.g., looking at the bright area in the middle. This modulation is due to the formation of a weak zigzag pattern (see Sec. III B). Note that the MFM contrast is only 1/3 of the contrast calculated for the type (I) sequence shown in Fig. 7(a).

Figure 7(c) presents the result for the type (III) domain pattern. The contrast is dominated by the interaction with the out-of-plane moments of the two diamond-shaped domains in the basal plane. As one is pointing out of the surface and the other into the surface [cf. Fig. 4(c)], the contrast is bright and dark, respectively. At the edges of the stripe, a weaker

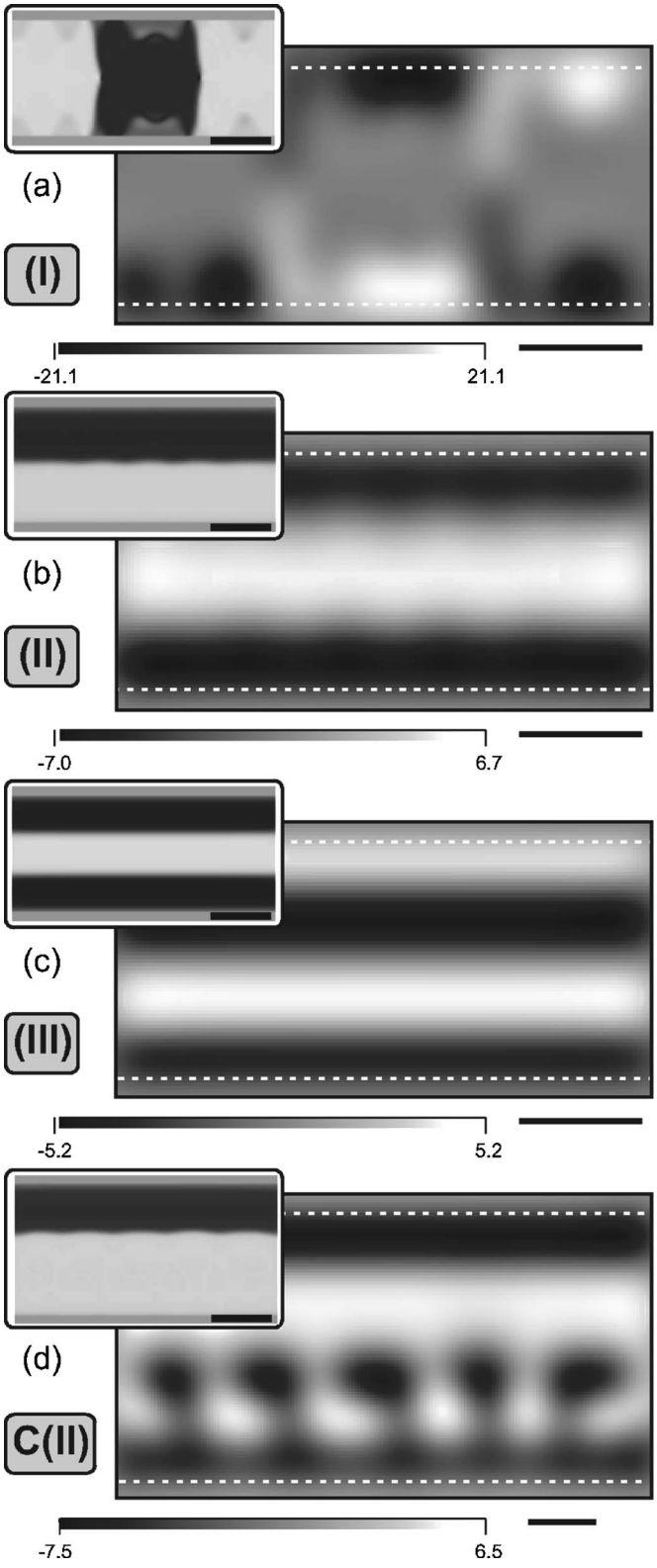

FIG. 7. MFM simulations of the standard domain types (I)–(III), shown in (a)–(c), respectively. The grayscale corresponds to the magnetic interaction force gradient in mN/m. The black bars correspond to 200 nm. The MFM contrast originating from the comblike domain structure is shown in (d). The dotted lines indicate the edges of the ferromagnetic stripe. The respective insets show the corresponding calculated XMCD-PEEM contrast.

contrast of the opposite sign is found. The magnitude of the force gradient is slightly smaller than in the case of the type (II) domain. Furthermore, the contrast is more confined to the actual stripe and no MFM signal is found outside the geometrical limits, as in the case of type (II) domains. The surface magnetization in all cases—corresponding to the XMCD-PEEM contrast—is in excellent agreement with the experimental image shown in Fig. 1.

Figure 8 depicts line scans of the simulated MFM contrast (shown in Fig. 7; sample temperature, 28 °C; thickness, 120 nm) along with experimental data extracted from Fig. 2 (sample temperature, 18 °C; thickness, 180 nm). The line scans were taken across the ferromagnetic stripes (along the *a* axis of MnAs). Note that the geometry of the simulated and measured stripe structure is different. In order to compare the results the stripe width is rescaled.

The simulated MFM line scan for the type (I) domain shown in Fig. 8(a) (open circles) is symmetrical for both attractive and repulsive forces. The simulated MFM data represent the MFM contrast obtained in the so-called lift mode, i.e., solely recording magnetically induced contrast by scanning on the known topography-induced path. The maximum magnetic interaction is right at the edges of the stripe and extends slightly beyond its boundaries. The experimentally obtained MFM curve [Fig. 8(a), solid squares], on the other hand, is asymmetric with respect to the sign of the interaction force. In particular, the measured attractive force peak is much broader than the one seen in the simulated curve. The origin of this discrepancy is the mode of operation of the MFM, where the phase shift is kept constant. As a result, in the case of an attractive interaction, the cantilever retracts farther away from the surface and the magnetically induced peak broadens. The missing repulsive dip, observed in the simulated contrast, is due to the van der Waals interaction which is stronger toward the surface. It has to be noted that the ratio between simulated and experimental values is kept the same for all plotted curves in Figs. 8 and 9.

For the type (II) domains, the simulated contrast generally agrees well with the measured MFM contrast [cf. Fig. 8(b)]. In detail, the measured contrast exhibits secondary maxima at the edges of the stripes which give rise to the white edges seen in Fig. 2. These edges only occur in case of repulsive interaction and are a result of the convolution of the topography-induced and magnetic interactions. The two line scans for the type (III) domain show excellent agreement. The central peak, which is due to an out-of-plane magnetized diamond domain in cross section, is equally broad in the simulated and measured MFM scan. In contrast, the neighboring trench, which is due to an oppositely magnetized diamond domain, is broader in the experimental scan compared to the simulated scan. Thus, it is likely that the assumed tip radius and coating thickness was slightly overestimated.

C. Results for the comblike domain pattern

The MFM contrast of the comblike domain pattern presented in Fig. 5 is shown in Fig. 7(d). This domain pattern, which gives rise to an asymmetric type (II) domain at the surface, leads to comblike patterns in the MFM contrast

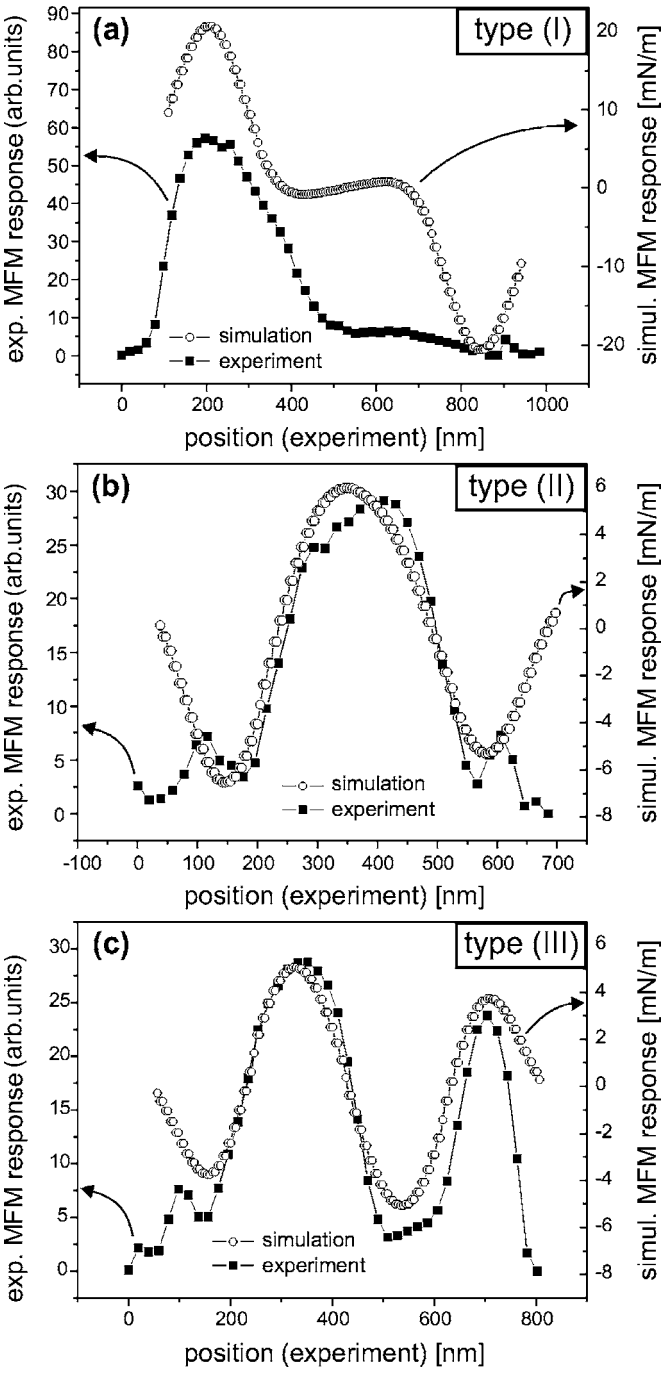

FIG. 8. Comparison of the simulated and measured MFM response (line scans) across ferromagnetic stripes showing (a) a type (I) domain, (b) a type (II) domain, and (c) a type (III) domain. The simulated MFM response is given in mN/m and the measured MFM response in arbitrary units (arb. units).

(bright). In correspondence with the related type (III) domains, a dark area is located close to the edge of the stripe. The dominant bright area is oriented along the stripe axis and asymmetrically shifted to the lower stripe edge. Its origin is, like for the type (II) and (III) domains in general, a diamond-like domain. From this area, hook-shaped features extend toward the upper edge of the stripe. These are connected to areas within the MnAs film that are showing out-of-plane

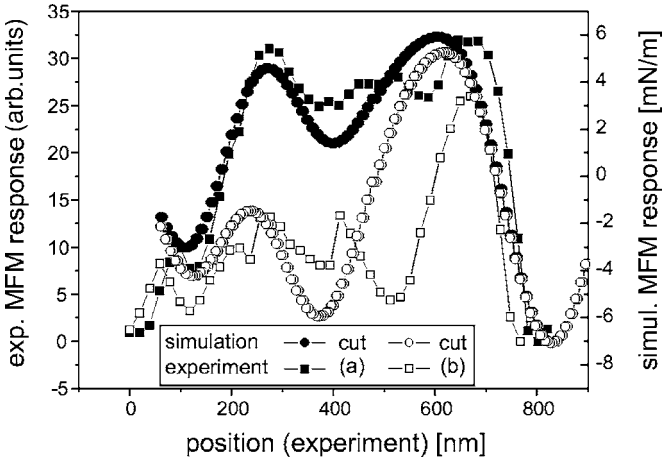

FIG. 9. Comparison of the simulated and measured MFM response (line scans) across a comblike domain structure [type (CII)]. The solid symbols represent a cut through an arm of the comb structure [cut (a)], and the open symbols a cut in between two arms [cut (b)], as indicated in Fig. 5.

magnetization components. In Fig. 5, these areas can be clearly identified. As for the ordinary type (II) domains, the magnitude of the magnetostatic tip-sample interaction is comparable. The simulated XMCD-PEEM contrast shows a type (II) domain on the surface.

Figure 9 shows experimental and simulated MFM line scans across the ferromagnetic stripe exhibiting a comblike domain structure. The first line scan is along the arm of the bright hook-shaped structure and the second line scan is in between two bright hook-shaped structures [cf. cut (a) and (b) in Fig. 5]. A remarkable qualitative agreement is found between the measured and simulated data. In general, the (a) scan (dark symbols) exhibits larger values than the (b) scan (bright symbols). On top of the cross-sectional diamond structure with an out-of-plane magnetization, the contrast is the same in the simulation for both cuts and very similar in the experiment. The fine structure along the (a) cut is clearly resolved in both experiment and simulation and the contrast ratios are in excellent agreement. In the (b) scan, the simulated features appear broader than the measured peaks, again pointing toward an overestimation of the tip dimensions in the simulation. The contrast ratio between the primary maximum (on the left) and the secondary maximum (on the right) agree very well, and the simulation reproduces the experimental data correctly.

V. DISCUSSION

In general, the results of the micromagnetic simulation and the experimentally determined surface magnetization agree qualitatively very well [cf. Fig. 3(b) (M_y component), Fig. 1 (projection of the magnetization onto the a axis $\parallel y$ axis), and the insets in Fig. 7]. All three domain types are found in both simulation and the XMCD-PEEM measurement. From the energies listed in Table I, it is clear that types (II) and (III) are equal in energy and the preferred domain configurations for the arrangement of the stripes. Neverthe-

less, type (I) domains are experimentally found both as extended structures and as an alternating sequence of oppositely magnetized domains. In this case, the domain statistics obtained from the two complementary methods differ. This is not surprising, since the origin of the type (I) domain—an *S* state, *C* state, or Landau state—cannot be determined by XMCD-PEEM imaging alone.

Comparing the experimental and simulated MFM contrast in Figs. 2(a) and 7, respectively, yields an excellent agreement. Not only does the simulation reproduce the contrast patterns qualitatively, but also the relative magnitudes of the stray fields are reproduced correctly. This is most easily seen in the case of the alternating type (I) domain sequence. The contrast due to this sequence governs the MFM image [cf. Fig. 2(a), right-hand side], in accordance with the calculated MFM contrast [cf. force gradient scale in Fig. 7(a)]. In fact, the force gradient is a factor of 3 larger than the response due to the other domain types. It is worth noting that the magnitude of the MFM contrast precisely follows the trend in the stray-field energies (E_{demag}): the MFM response decreases from type (I) over type (II) to type (III) such as 1:0.33:0.25 and the energies such as 1:0.32:0.26.

Another peculiar feature of the MFM image is a fine bright line [cf. 2(a), rectangle marking the type (II) domain]—approximately at the position of the phase boundary of α- and β-MnAs—which is not reproduced by the simulations. The reason for this feature is the convolution of the topography with the magnetic interaction, as discussed in Sec. IV. It has to be noted that, apart from the fine bright lines at the edges, the magnetic interaction dominates the topography-related interaction at the selected working height. As the force gradient is kept constant by the MFM, in regions of repulsive magnetic interaction the tip-sample distance is decreased, leading to an enhanced topography signal. This is exclusively found at the α-stripe edges where the magnetic interaction is repulsive [dark contrast, cf. Fig. 2(a)] and the topography gradient is maximum (2 nm in the case of a 180-nm-thick MnAs film). In the case of alternating type (I) domains, the fine feature is not seen in MEM images, as the stray field of the predominantly in-plane magnetized areas extends far beyond the boundary of the ferromagnetic stripe.

The remaining difference between the XMCD-PEEM and MFM images is the larger relative abundance of extended type (I) domains and also type (II) domains in the case of the surface-sensitive method.[26] This apparent discrepancy can be resolved by analyzing the comblike domain pattern in detail. As explained above, the discussed comblike structure C(II) gives rise to a type (II) domain on the surface [see Fig. 7(d)]. The underlying domain state is an asymmetric diamond state with an extending cross-tie wall. In addition to these structures, another comblike structure, termed C(I), is found in the MFM image in Fig. 2(a). It shows a bright contrast extending along the stripe right at one of its edges. From the edge, fingerlike bright features extend across the stripe. Their separation is comparable to the distance of the hooklike features found for C(II) domains. C(I) domains are thus a combination of an extended type (I) structure leading to bright and dark contrast at opposite edges of the stripe and a comblike pattern. The MFM contrast is obviously much smaller than typical for a type (I) domain sequence, ruling out the *C* and *S* states as the governing domain patterns in the basal plane. Instead, a Landau state can be held responsible for the observed contrast. First, it naturally leads to a smaller stray field in MFM. Second, the calculated Landau state shown in Fig. 3(d) exhibits a cross-tie wall, which was found to move across the width of the stripe, giving rise to the hook-shaped C(II) structures.

VI. CONCLUSIONS

In summary, we presented a comparative discussion of magnetic contrast seen by XMCD-PEEM and MFM using MnAs in the stripe phase as an example. Employing these two complementary micromagnetic imaging techniques, in conjunction with micromagnetic simulations, leads to a consistent micromagnetic picture of this materials system. In the cross-section of the wires, a number of metastable magnetization patterns are found that resemble the flux-closure patterns known from soft magnetic materials: the *C*, *S*, and Landau states [type (I) domains], the diamond state [type (II) domains], and the double-diamond state [type (III) domains]. By performing MFM simulations of these magnetization patterns, and by taking surface-sensitive XMCD-PEEM images into account, the simulated patterns can be largely confirmed. A deeper look into the distribution of stripe widths at a given temperature resulted in the discovery of two additional comblike patterns for wider α stripes. The C(I) state is related to the ordinary type (I) domain based on a Landau state, whereas the C(II) state is based on an asymmetric diamond state. Both states exhibit a widely stretched Néel wall which is stabilized by forming a cross-tie wall. As these states appear as type (I) and (II) domains on the surface, but as comblike domains in MFM, the remaining discrepancy in the domain count for both experimental methods can be resolved. MnAs on GaAs is thus a good example of the value of MFM data for the determination of the micromagnetic domain structure, when combined with advanced contrast simulations based on micromagnetic simulations.

ACKNOWLEDGMENTS

The authors want to thank C. Herrmann for the sample preparation, J. R. Mohanty for help with the MFM measurements, and K. H. Ploog for his continuous and generous support.

*Corresponding author. Electronic address: t.hesjedal@ece.uwaterloo.ca

[1] K. J. Kirk, S. McVitie, J. N. Chapman, and C. D. W. Wilkinson, J. Appl. Phys. **89**, 7174 (2001).

[2] R. P. Cowburn, D. K. Koltsov, A. O. Adeyeye, M. E. Welland, and D. M. Tricker, Phys. Rev. Lett. **83**, 1042 (1999).

[3] J. K. Ha, R. Hertel, and J. Kirschner, Phys. Rev. B **67**, 224432 (2003).
[4] G. A. Prinz, Science **250**, 1092 (1990).
[5] M. Tanaka, Semicond. Sci. Technol. **17**, 327 (2002).
[6] M. Ramsteiner, H. Y. Hao, A. Kawaharazuka, H. J. Zhu, M. Kästner, R. Hey, L. Däweritz, H. T. Grahn, and K. H. Ploog, Phys. Rev. B **66**, 081304(R) (2002).
[7] V. M. Kaganer, B. Jenichen, F. Schippan, W. Braun, L. Däweritz, and K. H. Ploog, Phys. Rev. B **66**, 045305 (2002).
[8] M. Kästner, C. Herrmann, L. Däweritz, and K. H. Ploog, J. Appl. Phys. **92**, 5711 (2002).
[9] It is still considered an open question whether β-MnAs is paramagnetic or antiferromagnetic. For a discussion see H. Yamaguchi, A. K. Das, A. Ney, T. Hesjedal, C. Pampuch, D. M. Schaadt, and R. Koch, Europhys. Lett. **72**, 479 (2005).
[10] C. Pampuch, A. K. Das, A. Ney, L. Däweritz, R. Koch, and K. H. Ploog, Phys. Rev. Lett. **91**, 147203 (2003).
[11] R. Engel-Herbert, J. Mohanty, A. Ney, T. Hesjedal, L. Däweritz, and K. H. Ploog, Appl. Phys. Lett. **84**, 1132 (2004).
[12] R. Engel-Herbert, T. Hesjedal, J. Mohanty, D. M. Schaadt, and K. H. Ploog, Phys. Rev. B **73**, 104441 (2006).
[13] R. Engel-Herbert, T. Hesjedal, J. Mohanty, D. M. Schaadt, and K. H. Ploog, J. Appl. Phys. **98**, 063909 (2005).
[14] M. Tanaka, J. P. Harbison, M. C. Park, Y. S. Park, T. Shin, and G. M. Rothberg, Appl. Phys. Lett. **65**, 1964 (1994).
[15] F. Schippan, G. Behme, L. Däweritz, K. H. Ploog, B. Dennis, K.-U. Neumann, and K. R. A. Ziebeck, J. Appl. Phys. **88**, 2766 (2000).
[16] R. W. De Blois and D. S. Rodbell, Phys. Rev. **130**, 1347 (1963).
[17] J. Lindner, T. Tolinski, K. Lenz, E. Kosubek, K. Baberschke, A. Ney, T. Hesjedal, C. Pampuch, R. Koch, L. Däweritz, and K. H. Ploog, J. Magn. Magn. Mater. **277**, 159 (2004).
[18] R. Engel-Herbert, D. M. Schaadt, S. Cherifi, E. Bauer, R. Belkhou, A. Locatelli, S. Heun, A. Pavlovska, J. Mohanty, K. H. Ploog, and T. Hesjedal, J. Magn. Magn. Mater. **305**, 457 (2006).
[19] E. Bauer, S. Cherifi, L. Daeweritz, M. Kaestner, S. Heun, and A. Locatelli, J. Vac. Sci. Technol. B **20**, 2539 (2002).
[20] G. Schütz, W. Wagner, W. Wilhelm, P. Kienle, R. Zeller, R. Frahm, and G. Materlik, Phys. Rev. Lett. **58**, 737 (1987).
[21] T. Schmidt, Microsc. Microanal. **9**, 122 (2003).
[22] A. Hubert and R. Schäfer, *Micromagnetic Domains* (Springer, Berlin, 1998).
[23] R. Engel-Herbert, A. Locatelli, S. Cherifi, D. M. Schaadt, J. Mohanty, K. H. Ploog, E. Bauer, R. Belkhou, S. Heun, A. Pavlovska, T. Leo, and T. Hesjedal, Appl. Phys. A: Mater. Sci. Process. **84**, 231 (2006).
[24] J. Mohanty, R. Engel-Herbert, and T. Hesjedal, Appl. Phys. A: Mater. Sci. Process. **81**, 1359 (2005).
[25] R. Engel-Herbert, D. M. Schaadt, and T. Hesjedal, J. Appl. Phys. **99**, 113905 (2006).
[26] It has to be noted that the thickness of the investigated films is not identical. As a matter of fact, this leads to a different domain statistics as the existence of, e.g., diamond states in the basal plane of MnAs is critically depending on the film thickness. Another factor determining the domain statistics is the magnetic and phase transition history of the samples, which is hard to reproduce in detail unless an *in situ* MFM would be employed.
[27] This temperature refers to the distribution of the MnAs phases in the phase coexistence regime. The micromagnetic simulation was performed at zero temperature, thus ingnoring the effects of thermal fluctuations.
[28] M. Tanaka, J. P. Harbison, M. C. Park, Y. S. Park, T. Shin, and G. M. Rothberg, J. Appl. Phys. **76**, 6278 (1994).
[29] L. Däwerwitz, L. Wan, B. Jenichen, C. Herrmann, J. Mohanty, A. Trampert, and K. H. Ploog, J. Appl. Phys. **96**, 5056 (2004).
[30] R. Engel-Herbert, Ph.D. thesis, Humboldt University, 2006.
[31] Narrower stripes were found to exhibit (extended) type (I) domains. Details can be found in Ref. 12.